Reducing the Noise Impact of Small Aircraft through Indirect Trajectory Optimization

Matthew B. Galles*
NASA Langley Research Center, Hampton, Virginia, 23681

Brett Newman[†]
Old Dominion University, Norfolk, Virginia, 23529

This research examined the feasibility of incorporating an acoustic metric into the optimization of an aircraft trajectory to reduce the noise experienced by an observer. The method investigated a perturbed path of an unmanned aerial system with specified boundary conditions on position and velocity while maintaining a nominal flight speed. An acoustic model based on Gutin's work was developed to estimate propeller noise as a function of flight parameters, propulsion characteristics, and spatial location. A trajectory was then optimized a priori to reduce the noise experienced by an observer. Multiple simulations were performed and results showed that integrating an acoustic metric into the path planning process could be used to reduce the noise impact on an observer with no perturbation to the nominal flight speed.

I. Nomenclature

Acronyms

BC	Boundary Condition
BPF	Blade Passage Frequency
DEP	Distributed Electric Propulsion
GL-10	Greased Lightning-10
OASPL	Overall Sound Pressure Level
PNM	Propeller Noise Model
RMS	Root-Mean-Square
SPL	Sound Pressure Level
UAM	Urban Air Mobility
UAS	Unmanned Aerial System
UAV	Unmanned Aerial Vehicle
VTOL	Vertical Takeoff and Landing

Greek Symbols

λ	$\in \mathbb{R}^4$, Lagrangian multiplier vector	
χ	Heading angle	(deg)
μ	Constraint multiplier function	
ν	Flight velocity constraint	(m/s)
Ω	Propeller speed	(rad/s)
ϑ	Directivity angle between observer and axis of propeller rotation	(rad)

Roman Symbols

$C(\boldsymbol{x}, \boldsymbol{u}, t)$	Constraint function	
$F(\lambda_0)$	Summation of squared final state errors	
$H(\boldsymbol{x}, \boldsymbol{u}, \lambda, t)$	Hamiltonian	
J	Performance index	
$J_{qn}(x)$	Bessel function of the first kind of order qn and argument x	
$L(\boldsymbol{u}, t)$	Lagrangian	
L_p	Sound pressure level	(dB re. 2×10^{-5} Pa)
M	Mach number of the aircraft	

---

*Research Aerospace Engineer, Structural Acoustics Branch, MS 463, Hampton, VA 23681, AIAA Member.
[†]Professor, Dept. of Mechanical & Aerospace Engineering, Old Dominion Univ., Norfolk, VA 23529, AIAA Associate Fellow.

M_e	Mach number at an effective propeller radius	
M_t	Mach number of the propeller tip	
N	Number of vehicle states	
N_p	Number of aircraft propellers	
P_{disc}	$= T/\pi R_t^2$, Pressure loading on the propeller disc	(Pa)
Q	Propeller torque	(m N)
$\mathbb{R}^n$	Real vector space consisting of an n-sized tuple	
R_e	Effective propeller radius, ranges from $0.7R_t$ to $0.8R_t$	(m)
R_t	Propeller tip radius	(m)
$S(\boldsymbol{x}, t)$	Vehicle state constraint function	
T	Propeller thrust	(N)
c	Speed of sound in air	(m/s)
$\boldsymbol{f}(\boldsymbol{x}, \boldsymbol{u}, t)$	System dynamics	
n	Number of propeller blades	
p_0	$= 2 \times 10^{-5}$, Reference sound pressure	(Pa)
p_{rms}	Root-mean-square sound pressure at an observer	(Pa)
q	Harmonic index	
r	Distance from center of propeller rotation to observer	(m)
$\boldsymbol{r}_{o/a}$	Position vector of the acoustic observer relative to aircraft	(m)
$\boldsymbol{u}$	$\in \mathbb{R}^2$, Control vector	
$\boldsymbol{v}_a$	Aircraft velocity vector	(m/s)
x	$= kR\sin\vartheta$, Bessel function argument	
$\boldsymbol{x}$	$\in \mathbb{R}^4$, State vector	

II. Introduction

URBAN AIR MOBILITY (UAM) could provide a solution to traffic issues in heavily congested cities and surrounding areas. To support the UAM market, a class of vehicles has been proposed that use rotors or a combination of rotors and propellers such as a distributed electric propulsion (DEP) system. As these vehicles will most likely operate near populated areas away from airports, it is important to develop technologies to mitigate the noise impact on communities.

Previous work by the authors showed that the flight control system could be augmented to modify flight speed to reduce the sound pressure level (SPL) of a vehicle without perturbing the nominal flight path [1]. Augmenting the flight control system in this way could create a rectilinear but variable speed trajectory such as the one shown in Fig. 1 starting at point A and ending at point B.

The objective of the current work is to modify the trajectory of a vehicle to reduce the SPL at an observer without perturbing the nominal flight speed. This work is a step toward developing a vehicle that considers its noise impact on the surrounding environment during a mission, i.e., an acoustically aware vehicle. An example of this mission is shown in Fig. 2, where a trajectory is presented to avoid acoustically sensitive areas; within one of these acoustically sensitive areas exists an acoustic observer. This trajectory avoids direct overflight of an acoustic observer and achieves certain departure and arrival conditions at points A and B. As sound pressure decays with distance from a noise source, the fundamental approach in this work modifies the trajectory to increase the distance between the source and acoustic observer to satisfy an SPL constraint. This approach could complement or provide an alternative solution to active noise cancellation or passive noise reduction to reduce observer noise.

There have been a few efforts to optimize a trajectory while considering an acoustic constraint. Recently, Ackerman and Gregory [2] developed an a priori trajectory generation framework based on Hermite interpolation using Bézier polynomials that incorporates an acoustic constraint. This method formulated the path, dynamic, and acoustic constraints as Bézier curves [3]. Their approach avoided discretization of the trajectory and constraint functions, which guaranteed feasibility of the optimized trajectory. The acoustic model used overall sound pressure level (OASPL) as the acoustic metric and scaled with propeller speed, distance to observer, and number of propeller blades. Ackerman and Gregory's method was computationally efficient and enabled near real-time path planning, but applied only to the acoustic model considered in Ref. [2], in which the acoustic constraint could be formulated as a rational polynomial. This formulation allowed the acoustic constraint to be represented as a Bézier curve, which was necessary for their optimization framework.

In 2019, Greenwood [4] proposed a method for rotorcraft trajectory optimization suitable for dynamic replanning, inspired by similar research in robotics, unmanned aerial vehicles (UAVs), and autonomous ground vehicles [5–7].
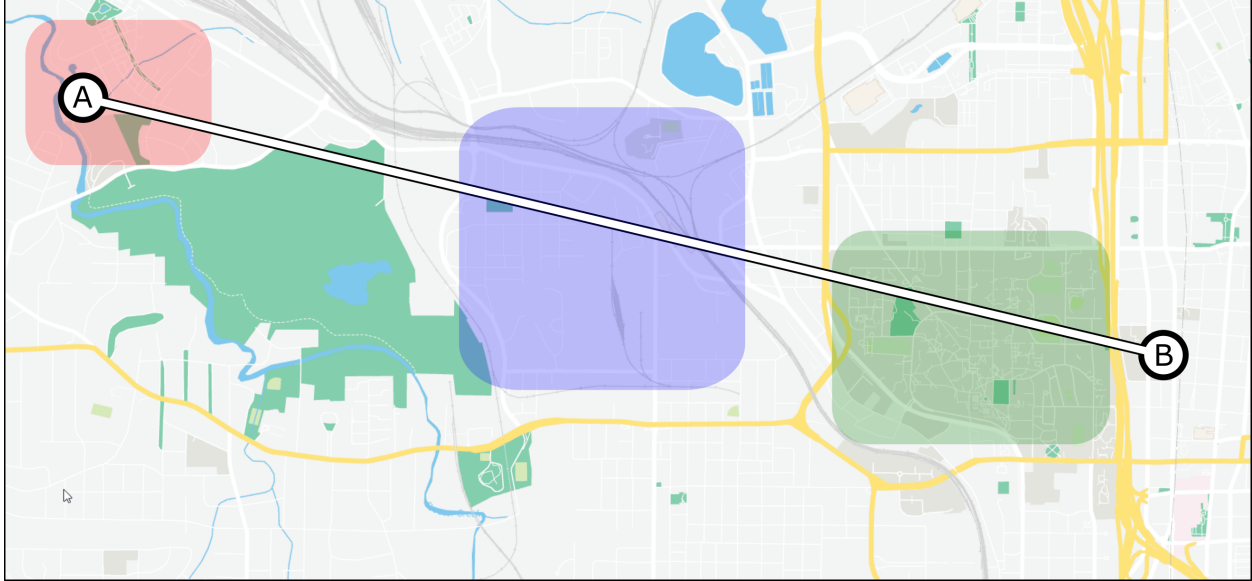
Fig. 1 Rectilinear Path with Variable Speed over Urban Community.

This method used a combinatorial optimization technique to determine the path of a rotorcraft around acoustically sensitive areas according to a defined acoustic cost. First, a large database of rotorcraft maneuver segments was generated and an acoustic cost for each segment was calculated using a semiempirical noise model. Then, individual maneuver segments were combined based on the total acoustic cost to form an optimal flight path. This method was computationally cheap, enabling near real-time dynamic replanning, but the optimality of the solution was constrained by the discretized nature of the combined maneuver segments. There is potential for reduced noise at acoustically sensitive areas with a continuous method that does not constrain the vehicle state at discrete locations, although likely at a higher computational cost.

Falck et al. [8] described an initial study in generating quadrotor trajectories using direct gradient-based optimization techniques. Their work coupled a six degree of freedom quadrotor model with an acoustic monopole model of constant sound power to track the SPL perceived by a ground observer during a flyover. In doing this, they created trajectories that did not violate limits placed on the SPL perceived by an observer. A potential limitation of this method is that the acoustic source is a low fidelity acoustic model that is not dependent on the vehicle state.

Where previous methods have used direct optimization or Bézier polynomials, this current work uses functional optimization, without prescribing the functional characteristics of the trajectory, to identify functions of time that minimize a performance index [9]. These functions of time constitute the vehicle trajectory and control inputs without assumptions of the type or class of curves that the aircraft will follow. The trajectory generation algorithm is a two-step process, in which the first step uses indirect optimization to calculate a specified-time trajectory with control effort as a performance index. Indirect optimization involves formulating the problem as a two-point boundary value problem, which is then solved to calculate a set of initial conditions that result in the desired final boundary conditions (BCs) [9]. The second step of the trajectory generation algorithm consists of an iterative procedure that modifies the previously calculated optimal trajectory using the flight duration as a degree of freedom to satisfy an acoustic constraint. This algorithm requires the equations that dictate the optimal conditions and results in a specified-time trajectory that is optimal with respect to control effort while constrained by an acoustic target. The result of the trajectory generation algorithm will be an optimal path, generated a priori, for a path-following controller to use during flight.

The paper is organized in the following sections. Section III describes the Propeller Noise Model developed for this work. Section IV presents the trajectory optimization algorithm. Section V provides simulations performed to test the proposed algorithm and corresponding results. Conclusions and opportunities for future work are presented in §VI.

III. Propeller Noise Model Development

A sound metric and a noise model are necessary to incorporate noise into the trajectory optimization algorithm. In this section, the vehicle of interest, the sound metric, the Propeller Noise Model (PNM), and implementation of the PNM will be described.
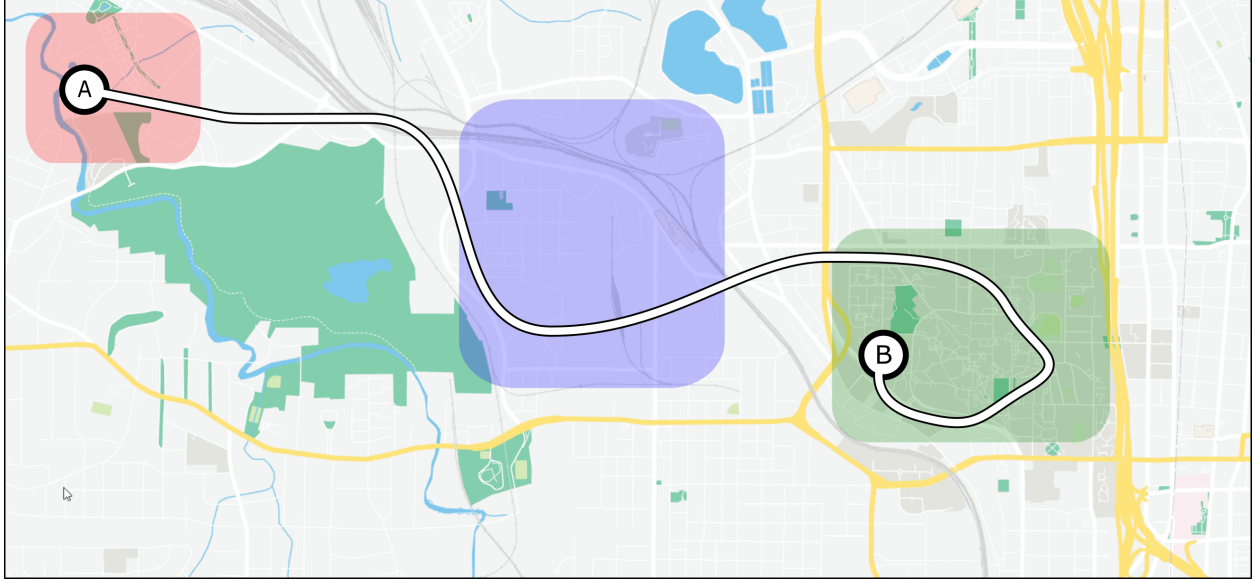
Fig. 2 Curvilinear Path with Constant Speed over Urban Community.

A. Vehicle

The vehicle chosen for the present work is the Greased Lightning-10 (GL-10), developed and built at the NASA Langley Research Center [10, 11]. The GL-10 is a ten propeller, 50% scale DEP vehicle used to prototype flight controls for vertical takeoff and landing (VTOL) aircraft. A nonlinear dynamics model developed from wind tunnel testing [12], a flight control system, and a path-following controller [13] were available for this aircraft and were previously implemented in Simulink [14]. The GL-10 uses three-bladed, 16.0×8.0 inch folding propellers and the propeller arrangement on the GL-10 has been previously described by Pascioni and Rizzi [15].

B. Propeller Noise Model

As the vehicle model for this work is propeller driven, an estimation of propeller noise experienced by an observer is required. Gutin was the first to estimate propeller noise based on the steady thrust and torque loads on a propeller; his relationship will be used for a simple estimation of propeller noise [16]. Although limited in complexity, the Gutin equation is a good candidate for a low fidelity model as it has been shown to provide good results for the first few harmonics of the blade passage frequency (BPF) [17]. Additionally, the Gutin equation is an analytical model that can easily be implemented in simulation.

According to Gutin [16], this model should only be used for stationary noise estimation without forward flight; however, literature suggests that it can be acceptable for low speed forward flight when the vehicle speed is small compared to the speed of sound [18]. This simple model was deemed acceptable due to the low propeller tip speeds in this work [19, 20]. Sources of noise not considered in the Gutin formulation are: steady thickness noise, arising from the displaced air, steady nonlinear quadrupole terms, arising from inviscid flow near the surface of the propeller blade, and unsteady noise due to angle of attack or broadband noise [20, 21].

Gutin pressure constitutes the PNM for the trajectory simulation, however, the thrust and torque terms have been substituted out in favor of a formula independent of the torque. Thrust and torque are not readily available from the aircraft simulation, but rather will be derived from known quantities. Instead of using the relationship given by Ref. [16], an engineering form based on Theodorsen and Regier [18] is used, which yields the root-mean-square (RMS) pressure as

$$p_{rms}(P_{disc}, r, M_t, M, M_e, \vartheta) = \frac{P_{\text{disc}}}{2\sqrt{2}} \frac{R_t}{r} M_t \left(\frac{M}{M_e^2} - \cos \vartheta \right) q n J_{qn} \left(q n M_e \sin \vartheta \right), \tag{1}$$

with the propeller disc pressure given as

$$P_{\text{disc}} = \frac{T}{\pi R_t^2}, \tag{2}$$

in which T is the propeller thrust, R_t is the propeller tip radius, r is the observer distance, M_t is the propeller tip Mach number, M is the vehicle Mach number, M_e is the Mach number of the effective propeller radius (which is $0.75R_t$), ϑ is the directivity angle, q is the harmonic index, and n is the number of propeller blades. Figure 3 shows that the propeller rotates about the x-axis at a rate of Ω, r lies at an angle ϑ away from the x-axis,[†] and θ lies in the azimuthal plane, in which positive θ is in the direction of the propeller rotation.

The directivity angle is calculated using the dot product between the observer position vector and the aircraft velocity vector,

$$\vartheta = \arccos \frac{\mathbf{v}_a \cdot \mathbf{r}_{o/a}}{|\mathbf{v}_a||\mathbf{r}_{o/a}|}, \tag{3}$$

Fig. 3 Gutin Model Propeller Geometry.[*]

in which $\mathbf{v}_a$ is the aircraft velocity vector expressed in the inertial frame, given by

$$\mathbf{v}_a = \begin{bmatrix} \dot{x}(t) & \dot{y}(t) & \dot{z}(t) \end{bmatrix}, \tag{4}$$

and is in line with the propeller's axis of rotation. The relative position of the observer to the aircraft is $\mathbf{r}_{o/a}$ and taking the norm of $\mathbf{r}_{o/a}$ yields the distance to the observer from the center of the propeller, r.

To provide a conservative estimate of the observer SPL, uniform directivity is assumed using the angle at which maximum SPL occurs. This modification simplified the PNM and reduced the trajectory computation time. Figure 4 shows a polar plot of the SPL as a function of the directivity angle, calculated using Eqs. (1) and (6), experienced by an observer that is 2 m away from the propeller of the GL-10 flying at 30 m/s. As Gutin does not account for broadband noise, Eqs. (1) and (6) estimate 0 dB at 0° and 180° in the figure; this is acceptable because the observer is not in line with the propeller axis [16, 19]. Observe that the maximum SPL occurs at 0.6π rad (108° in Fig. 4) from the propeller axis. Substituting the maximum SPL angle into Eq. (1) yields

$$p^*_{rms}(P_{disc}, r, M_t, M, M_e) = \frac{P_{\text{disc}}}{2\sqrt{2}} \frac{R_t}{r} M_t \left(\frac{M}{M_e^2} - \cos 0.6\pi \right) qn J_{qn} \left(qn M_e \sin 0.6\pi \right). \tag{5}$$

A detailed comparison between the variable directivity and uniform directivity PNMs can be found in Ref. [23]. The acoustic model provides an estimate of the observer SPL as a result of one GL-10 propeller, given by

$$L_p = 20 \log_{10} \left(\frac{p^*_{rms}}{p_0} \right), \tag{6}$$

in which L_p is the observer SPL and p_0 is the reference pressure. As the propellers are presumed to act as incoherent noise sources, a term is simply added to account for the additional GL-10 propellers. Thus, the new acoustic model is

$$L_p = 20 \log_{10} \left(\frac{p^*_{rms}}{p_0} \right) + 10 \log_{10} \left(N_p \right), \tag{7}$$

in which N_p is the number of propellers on the aircraft. Multiplying the sound pressure by the number of propellers reduced the computation time and simplified the PNM. For the simulations performed in this current work, the propeller noise model comprising Eqs. (5) and (7) was used.
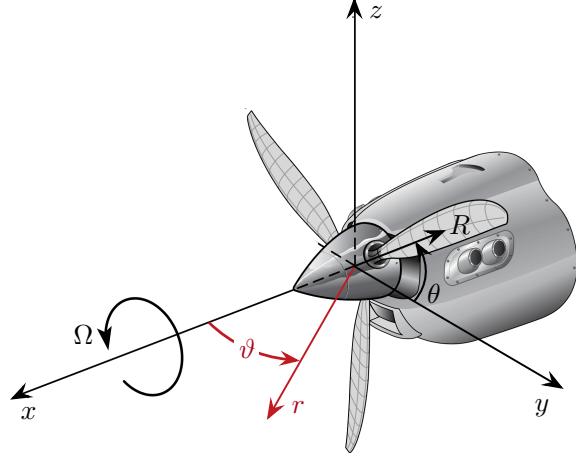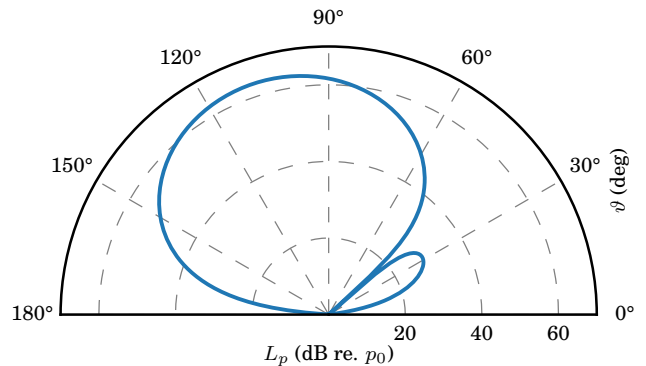

Fig. 4 Sound Pressure Level vs. Directivity Angle Between the Propeller Axis and the Observer.

---

[*]Figure modified from Zorumski and Weir [22].

[†]The observer position, $\mathbf{r}_{o/a}$, does not necessarily lie in the x-y plane.

5

IV. Optimal Trajectory Development

In this section, a method to modify the aircraft trajectory to satisfy an acoustic constraint at an observer without perturbing the nominal flight velocity is described. After an overview of the path generation process is presented, equations for optimality will be developed for a specified-time trajectory. Finally, incorporation of an acoustic constraint into the optimization process will be presented.

A. Overview

A flow chart of the path generation process is presented in Fig. 5. This process contains: (i) an optimization routine to determine a specified-time trajectory between starting and ending points subject to BCs and (ii) an iterative algorithm to modify the flight time based on an SPL constraint. There exists a unique flight path for a specified flight time, constrained by the system dynamics ($\dot{\boldsymbol{x}}$), that results in an optimal trajectory. For the current work, a trajectory was considered optimal if the control effort (the performance index) was minimized. Initial flight time and BCs are supplied to the optimization routine. Increasing the flight time forces the trajectory to deviate from a minimum-time trajectory, which curves the flight path away from the observer. This curved flight path is what provides the capability to avoid an acoustically sensitive area. Since flight time is a degree of freedom, the iterative algorithm increases the flight time if the observer SPL is too high; conversely, the algorithm decreases the flight time if the observer SPL is too low. The iterative algorithm ends when the desired observer SPL constraint is satisfied with a defined tolerance or an iteration limit is reached.
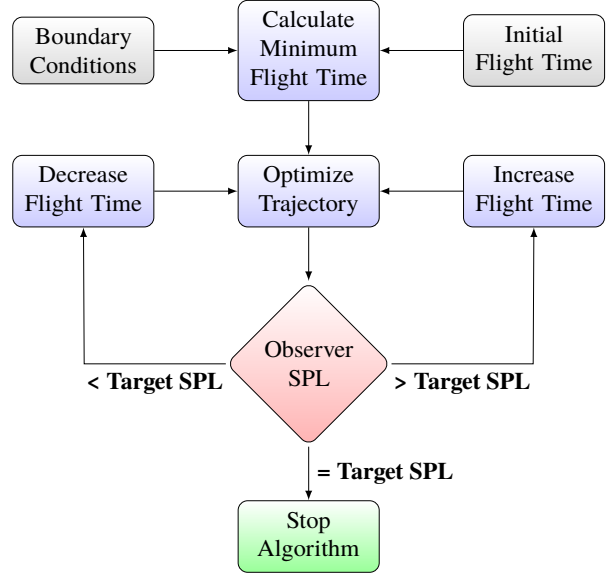

Fig. 5   Path Planning Flow Chart.

B. Equations for Optimality

The indirect optimization method used in the current work is based on Bryson and Ho [9] and Pontryagin et al. [24]. The dynamic equations for optimality are called the state and costate (or adjoint) equations, and have been previously derived in the literature for a one-dimensional case [25]. Additionally necessary for the current work is a constraint equation, used to constrain the flight velocity to a nominal value. A scalar auxiliary function known as the Hamiltonian binds the performance index to the state, costate, and constraint equations. The Hamiltonian, originally constructed for Pontryagin's maximum principle, is necessary to derive the costate equations [9, 24]. In this subsection, the state, costate, and constraint equations for a two-dimensional vehicle point mass model will be presented, which, when combined with a method to determine the appropriate initial conditions, will be used to calculate the optimal trajectory.

1. Dynamic System

As the altitude is assumed constant, the vehicle position is described by horizontal coordinates x and y. The vehicle state can be represented by

$$\boldsymbol{x} = \begin{bmatrix} x(t) & y(t) & \dot{x}(t) & \dot{y}(t) \end{bmatrix}^T = \begin{bmatrix} x_1 & x_2 & x_3 & x_4 \end{bmatrix}^T, \tag{8}$$

in which $\boldsymbol{x} \in \mathbb{R}^4$ is a state vector, (x_1, x_2) are the vehicle positions, and (x_3, x_4) are the flight velocities. The control vector input to the system, $\boldsymbol{u} \in \mathbb{R}^2$, can be represented by the acceleration of the vehicle as

$$\boldsymbol{u} = \begin{bmatrix} \ddot{x}(t) & \ddot{y}(t) \end{bmatrix}^T = \begin{bmatrix} u_1 & u_2 \end{bmatrix}^T. \tag{9}$$

The system dynamics are described by the state equation, which comprises the following linear differential equations

$$\dot{\boldsymbol{x}} = \boldsymbol{f}(\boldsymbol{x}, \boldsymbol{u}, t) = A\boldsymbol{x} + B\boldsymbol{u}, \tag{10}$$

for the time period $t_0 \leq t \leq t_f$. The system is subject to BCs on initial and final states, x_0 and x_f, respectively, and a speed constraint of

$$x_3{}^2 + x_4{}^2 = v^2, \tag{11}$$

in which v is the specified flight speed.

2. Performance Index

To create an optimal trajectory, it is desired to find the control inputs, u, as functions of time that minimize the equation

$$J = \int_{t_0}^{t_f} L(u,t)\,dt, \tag{12}$$

in which J is the scalar performance index from initial to final time and L is the Lagrangian subject to the BCs and state constraints of the system. The desired objective is to minimize the control effort of the aircraft, which means the Lagrangian of this system is

$$L(u,t) = \frac{1}{2}u^T u, \tag{13}$$

resulting in the objective function

$$J = \frac{1}{2}\int_{t_0}^{t_f}(u_1^2 + u_2^2)\,dt. \tag{14}$$

3. State, Costate, and Constraint Equations

To derive the state, costate, and constraint equations for the optimal control problem presented in §IV.B.1 and §IV.B.2, a function known as the Hamiltonian will be used. The Hamiltonian, a scalar value, is defined as

$$H(x,u,\lambda,t) = L(u,t) + \lambda^T f(x,u,t) + \mu C(x,u,t), \tag{15}$$

in which $\lambda \in \mathbb{R}^4$ is the Lagrangian multiplier vector, defined as

$$\lambda = \begin{bmatrix} \lambda_1(t) & \lambda_2(t) & \lambda_3(t) & \lambda_4(t) \end{bmatrix}^T, \tag{16}$$

μ is the constraint multiplier function and C is the constraint function on the state and control variables. In this problem, only a constraint on the state variables exists, which, from Eq. (11), is given by

$$S(x,t) = x_3{}^2 + x_4{}^2 - v^2, \tag{17}$$

in which v is the flight velocity constraint of 30 m/s. The constraint function, $C(x,u,t)$, is related to Eq. (17) by[‡]

$$C(x,u,t) = \frac{dS}{dt} = \frac{\partial S}{\partial t} + \frac{\partial S}{\partial x}^T f(x,u,t). \tag{18}$$

As the state constraint is constant, the total time derivative of the state constraint in Eq. (18) is set to zero, from which the final constraint equation can be derived:

$$0 = x_3 u_1 + x_4 u_2. \tag{19}$$

From the constraint equation and the Hamiltonian, respectively, Eqs. (19) and (15), the following equations of optimality can be derived:

$$
\begin{array}{lll}
\mu = -\frac{x_3\lambda_3 + x_4\lambda_4}{x_3{}^2 + x_4{}^2} & \dot{x}_1 = x_3 & \dot{\lambda}_1 = 0 \\
u_1 = -\lambda_3 - x_3\mu & \dot{x}_2 = x_4 & \dot{\lambda}_2 = 0 \\
u_2 = -\lambda_4 - x_4\mu & \dot{x}_3 = u_1 & \dot{\lambda}_3 = -\lambda_1 - \dot{x}_3\mu \\
& \dot{x}_4 = u_2 & \dot{\lambda}_4 = -\lambda_2 - \dot{x}_4\mu.
\end{array}
\tag{20}
$$

Note that when μ equals zero, these governing equations collapse to the equations for optimality without a velocity constraint. A full derivation of the constraint equation and equations for optimality, Eqs. (19) and (20), can be found in Ref. [23].

[‡]Section 3.3 of Bryson and Ho [9].

4. Solving for the Optimal Trajectory

To calculate the initial optimal trajectory, first a conservative estimate of required flight time based on the distance between the initial and final BCs and aircraft velocity is calculated. Next, the initial Lagrangian multipliers required to achieve the desired final BCs are needed; to calculate these initial values, the following nonlinear least squares problem is posed:

$$F(\lambda_0) = \sum_{i=1}^{N} \left\| x_i(t_f) - x_{i,f} \right\|^2 .$$ (21)

A function of the initial Lagrangian multipliers, $F(\lambda_0)$, is based on the output of a Runge-Kutta integration, in which $\lambda_0 = \lambda(t_0)$ is the initial Lagrangian multiplier vector, $x_i(t_f)$ is the simulated final ith state of the aircraft, $x_{i,f}$ is the desired final ith state, and N is the number of states. A Levenburg-Marquardt algorithm is used to solve this system for the initial Lagrangian multipliers that result in the desired final BCs. Note that the final state BC error in Eq. (21) can be reduced precisely to zero. After solving for the initial Lagrangian multipliers, the dynamic equations in Eq. (20) are integrated with time to generate the optimal trajectory. After generating this trajectory that satisfies all appropriate BCs, the flight time is reduced and the process is repeated until a trajectory is generated that takes the minimum amount of time. The resulting minimum-time optimal trajectory describes the vehicle states and control inputs as functions of time. Determination of this trajectory is fully contained within the "calculate minimum flight time" block (shown in Fig. 5) and passes the minimum time to the optimize trajectory block .

C. Acoustic Constraint Incorporation

Once the initial optimal trajectory is determined, the maximum observer SPL during this flight is computed and used as a baseline value. Then, a desired SPL reduction at the observer is set. If the SPL reduction is not satisfied, then the flight duration is increased and the optimization is repeated. Increasing the flight duration forces the flight trajectory to curve away from the acoustic observer with a corresponding reduction in SPL at the observer. Note that the trajectory optimization is independent of the acoustic state, and that incorporating the acoustic constraint is an additional step, as shown in Fig. 5. If the SPL reduction is satisfied, then the flight duration is reduced to see if a shorter flight trajectory can be found that satisfies the SPL target. If the specified time is so short that no solution can be found, then the time is increased. Adaptive gain logic is included to reduce the change in flight duration if a smaller change in SPL is necessary. This iterative process continues until either the desired SPL reduction is met with a tolerance of 0.25 dB or 25 iterations are reached.

V. Simulation Results

This section will present the results of simulations performed using the algorithm developed to optimize a trajectory using the PNM. First, the nominal trajectory is described. Then, results of simulations to reduce observer SPL from the baseline value will be presented, analyzed, and compared.

A. Nominal Trajectory

To analyze the effectiveness of incorporating the PNM into the trajectory optimization algorithm, it is necessary to first define a baseline flight segment from which all simulations will be performed. The initial and final BCs for the flight segment are

$$x_0 = \begin{bmatrix} 0 & 0 & \nu \cos \chi_0 & \nu \sin \chi_0 \end{bmatrix}^T \text{ (m, m/s)} ,$$ (22)

$$x_f = \begin{bmatrix} 1000 & 200 & \nu \cos \chi_f & \nu \sin \chi_f \end{bmatrix}^T \text{ (m, m/s)} ,$$ (23)

in which ν is the nominal flight speed of 30 m/s, χ_0 is the initial heading angle of $0°$, and χ_f is the final heading angle of $0°$. An acoustic observer is placed at (500, 100) m on the ground, as shown in Fig. 6. To analyze the acoustic effects on the ground plane, the area shown in Fig. 6 is divided into a grid of 1500 evenly spaced points. The PNM is used to calculate the SPL at every time step and grid point on the ground plane based on the aircraft flying at a constant altitude of 30 m. The flight duration for a minimum-time and minimum control effort trajectory was 34 s, which corresponds to the trajectory shown in Fig. 6. The ground contour plot in Fig. 6 shows the maximum SPL at every grid point during the flight segment and has a color bar range of 25 dB (blue) to 52 dB (red). Note that the trajectory depends on the BCs and the flight duration may change for other initial and final states. The trajectory shown in Fig. 6 will henceforth be referred to as the nominal trajectory.
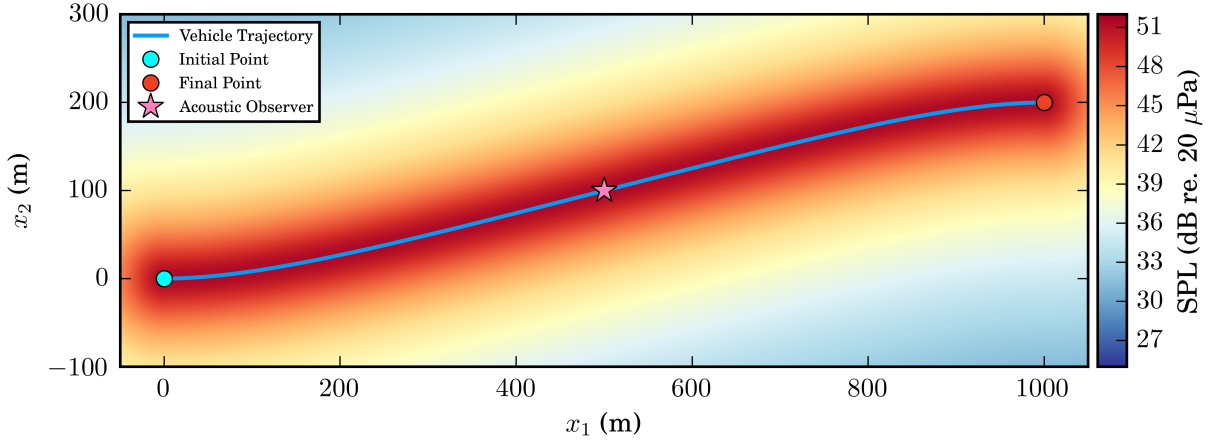
Fig. 6   Nominal Mininum-Time Trajectory with Ground Contour Plot of the Maximum SPL.

B. Simulations

Results of the nominal trajectory and five noise reduction simulations are presented in Table 1; respective trajectories are plotted in Fig. 7. These results include the desired maximum observer SPL reduction ($\Delta L_{\text{max, desired}}$), calculated maximum SPL (L_{max}), maximum SPL reduction achieved (ΔL_{max}), flight duration (t_f), and change in flight duration from the nominal (Δt_f).

The nominal trajectory corresponds to the first row of Table 1 and the blue trajectory in Fig. 7, in which the vehicle flew directly over the acoustic observer. This trajectory resulted in a maximum SPL at the observer of 51 dB and a flight duration of 34 s. As the desired maximum SPL was reduced in subsequent simulations, the iterative algorithm increased the flight time, thereby forcing the trajectory

Fig. 7   Trajectories with Various Maximum Sound Pressure Levels at an Observer.

to curve away from the observer and decreasing the maximum observer SPL. This trend is apparent in Table 1; as the flight times in columns 4 and 5 increase, the maximum observer SPL decreases for most of the simulations presented.

Results for a 15 dB reduction in maximum observer SPL are shown in the 4th row of Table 1 and correspond to the red trajectory in Fig. 7. To satisfy the noise reduction goal, the iterative algorithm increased the flight time by 2.63 s, creating a trajectory that curved away from the observer. This curved trajectory resulted in the maximum SPL contour shown in Fig. 8.

The results for a 20 dB reduction in maximum observer SPL are presented in the 5th row of Table 1 and the purple trajectory in Fig. 7. The actual reduction in observer SPL was the desired 20 dB with an increased flight duration of 13 s. Observe in Fig. 7 that the trajectory curved much further away from the acoustic observer when compared to the 5, 10, and 15 dB reduction trajectories. The ground contour plot (see Fig. 9) suggests that the maximum observer SPL was a result of the vehicle flying closer to the acoustic observer to satisfy the final BCs. Evidence to support this suggestion is presented below.

The trajectory generation process worked well for the previous cases, but failed to satisfy the BCs and the acoustic constraint when attempting to reduce the maximum observer SPL by 25 dB, which corresponds to the 6th row of Table 1 and the brown trajectory in Fig. 7. The actual maximum SPL reduction in this simulation was 20 dB and the flight duration increased by 33 s. Observe in Fig. 10 that the maximum SPL at the acoustic observer was due to the vehicle operating near the point $(800, 0)$ m to satisfy the final BCs. The optimization algorithm attempted to calculate a trajectory
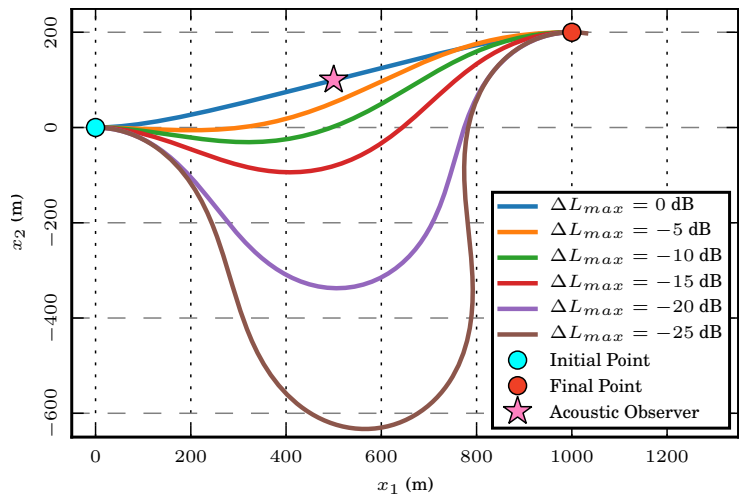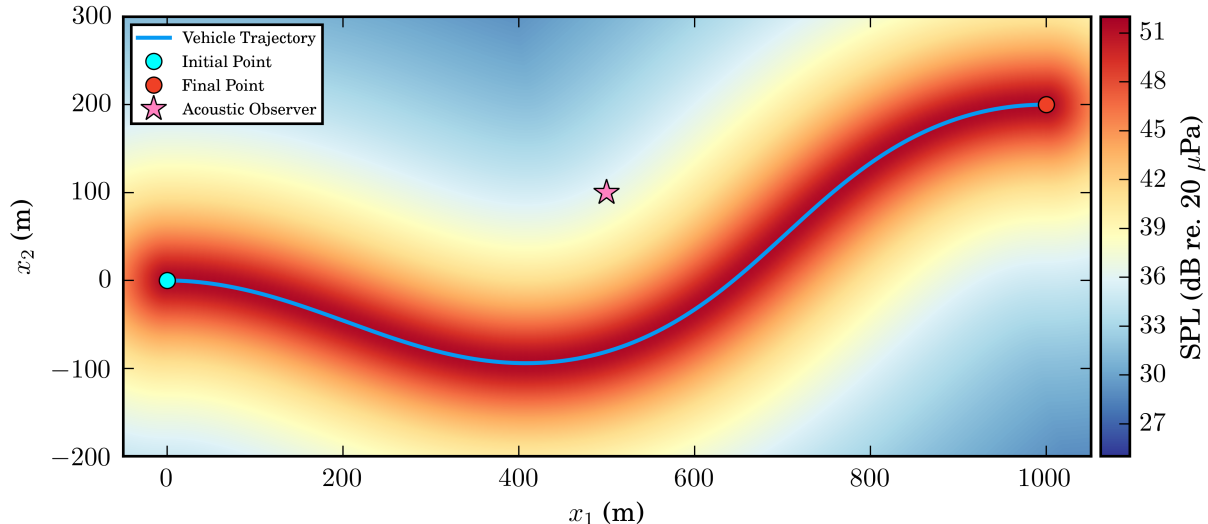
9

Fig. 8 Optimal Trajectory and Maximum SPL Contour for Desired Reduction of 15 dB at the Observer.

that would satisfy the acoustic constraint, but the process could not find a solution within the 25-iteration limit described in §IV.C. As a result, the process failed to generate a trajectory that satisfied both the time constraint and the final BCs. The trajectory solution at the 25th iteration, shown in Fig. 10, extended past the final point on the flight path. Increasing the 25-iteration limit only increased the flight duration, which was demonstrated in Ref. [23]. In this scenario, curving the trajectory away from the acoustic observer provided no further acoustic benefit and only resulted in increased flight time.

Table 1 Summary of Attempts to Reduce Observer Noise.

$\Delta L_{max, \text{ desired}}$ (dB re. p_0)	L_{max} (dB re. p_0)	ΔL_{max} (dB re. p_0)	t_f (sec)	Δt_f (sec)
0	51.42	0	34.05	0
-5	46.47	-4.95	34.49	0.44
-10	41.41	-10.01	35.02	0.97
-15	36.47	-14.95	36.68	2.63
-20	31.63	-19.79	47.49	13.44
-25	31.44	-19.98	67.49	33.44

VI. Conclusions and Future Work

This paper investigated incorporating acoustics into the path planning process with the objective of reducing observer noise during a flyby event. To meet this objective, a simple Propeller Noise Model was combined with a two-dimensional aircraft dynamics model to study trajectory optimization with an acoustic constraint on the ground. The generated trajectories minimized control effort and flight time to destination with a nominal flight speed. Six simulations were studied; these included a nominal, minimum-time flight path, plus five trajectories with increasing levels of noise reduction at a ground observer. The method successfully generated trajectories that satisfied the acoustic constraint for four of the five cases. In the fifth case, the optimization process could not generate a trajectory that satisfied both the acoustic constraint and the boundary conditions on the flight path.

The approach presented in this paper had limitations, some of which could be addressed in future work. It is difficult to incorporate an acoustic model directly into the cost function of the optimization framework developed here for a number of reasons. First, indirect optimization requires derivation of the differential equations that govern the change in both Lagrangian multipliers and state variables throughout the simulation. Second, a derivation of the state, costate, and constraint equations is required for each acoustic model used due to the differentiation of the cost function and acoustic model with respect to time and states. Finally, this issue is compounded as more complicated (and potentially more realistic) acoustic models are used. The present approach did not incorporate the acoustic model in the performance index, but rather included it in an iterative algorithm outside of the trajectory optimization routine.

While there are certain limitations to the work presented, this investigation demonstrated the capability that acoustics can be considered during the path planning process when calculating an optimized trajectory that minimizes control effort and time to destination for constant speed flight.

Future work will include incorporating higher fidelity acoustic models into the trajectory optimization framework. Additionally, direct optimization could be used to embed the acoustic model directly into the optimal control theory. This approach may allow for a more direct trajectory while satisfying acoustic constraints, thus reducing flight time.
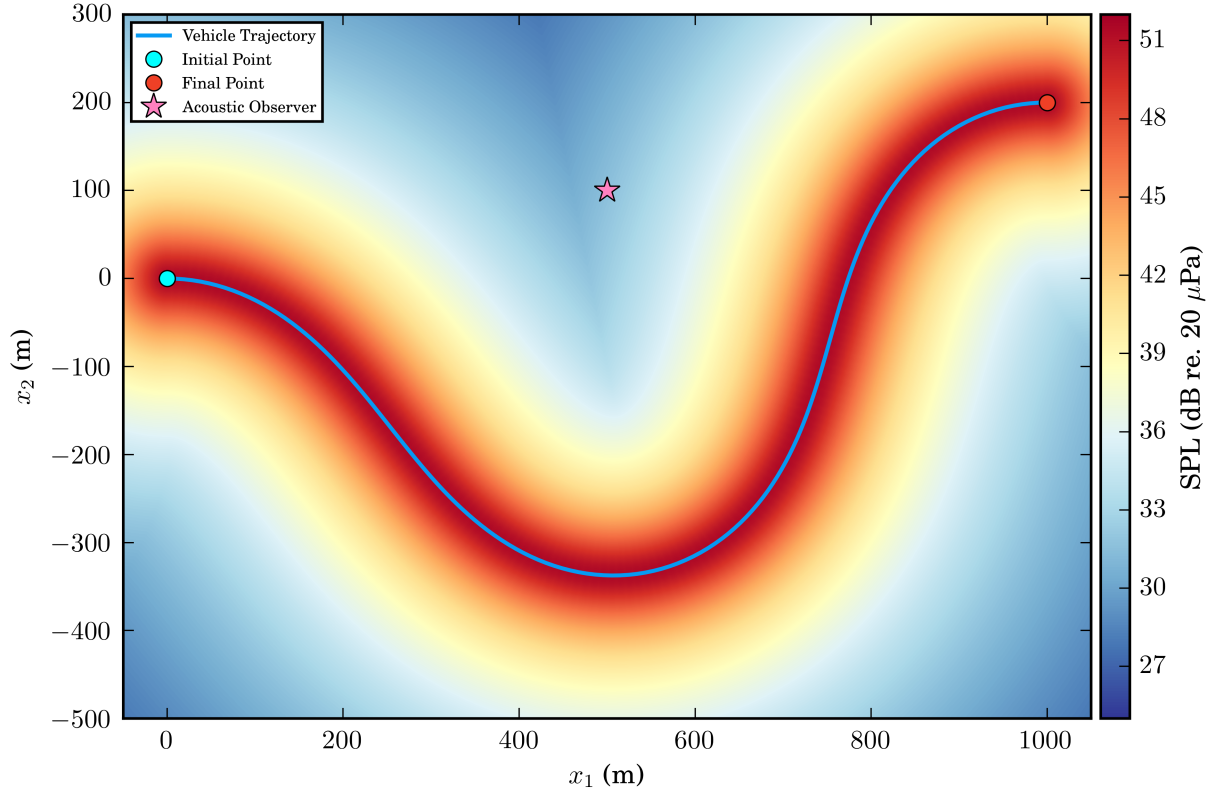
Fig. 9 Optimal Trajectory and Maximum SPL Contour for Desired Reduction of 20 dB at the Observer.

Acknowledgments

References

[1] Galles, M. B., Schiller, N. H., Ackerman, K. A., and Newman, B., "Feedback Control of Flight Speed to Reduce Unmanned Aerial System Noise," *2018 AIAA/CEAS Aeroacoustics Conference*, AIAA Aviation Forum, Atlanta, GA, June 2018. doi:10.2514/6.2018-2950, AIAA 2018–2950.

[2] Ackerman, K. A., and Gregory, I. M., "Trajectory Generation for Noise-Constrained Autonomous Flight Operations," *2020 AIAA Scitech Forum*, AIAA, Orlando, FL, Jan. 2020. doi:10.2514/6.2020-0978, AIAA 2020-0978.

[3] Choe, R., Puig-Navarro, J., Cichella, V., Xargay, E., and Hovakimyan, N., "Cooperative Trajectory Generation Using Pythagorean Hodograph Bézier Curves," *Journal of Guidance, Control, and Dynamics*, Vol. 39, No. 8, Aug. 2016, pp. 1744–1763. doi:10.2514/1.G001531.

[4] Greenwood, E., "Dynamic Replanning of Low Noise Rotorcraft Operations," *Vertical Flight Society 75th Annual Forum & Technology Display*, Vertical Flight Society, Philadelphia, PA, May 2019.

[5] Brumitt, B. L., and Stentz, A., "Dynamic Mission Planning for Multiple Mobile Robots," *1996 IEEE International Conference on Robotics and Automation*, IEEE, Minneapolis, MN, Apr. 1996, pp. 2396–2401. doi:10.1109/ROBOT.1996.506522.
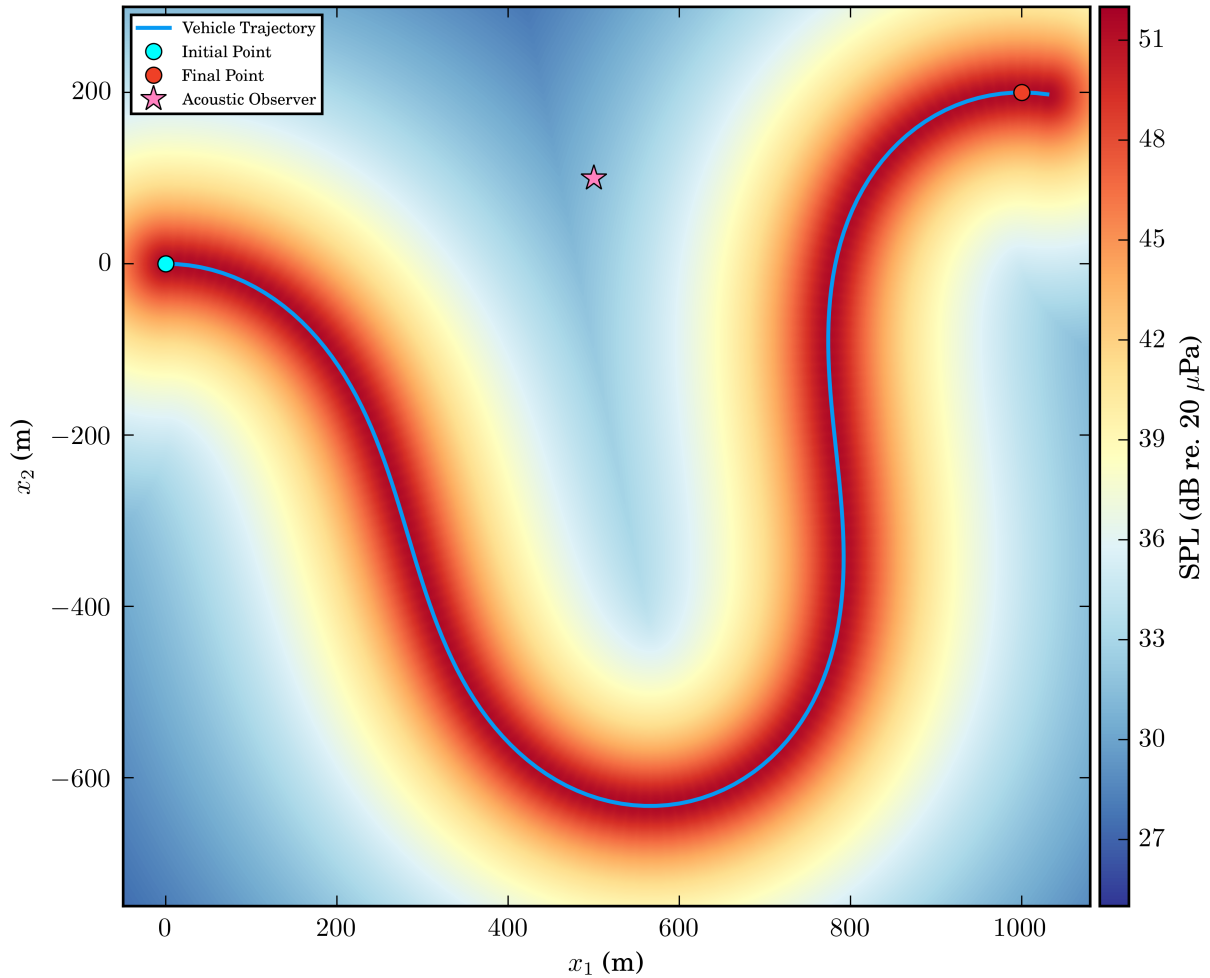
Fig. 10 Trajectory and Maximum SPL Contour Plot for Failed 25 dB Reduction Attempt.

[6] De Filippis, L., Guglieri, G., and Quagliotti, F., "Path Planning Strategies for UAVS in 3D Environments," *Journal of Intelligent & Robotic Systems*, Vol. 65, No. 1-4, Jan. 2012, pp. 247–264.
doi:10.1007/s10846-011-9568-2.

[7] Li, X., Sun, Z., Cao, D., Liu, D., and He, H., "Development of a New Integrated Local Trajectory Planning and Tracking Control Framework for Autonomous Ground Vehicles," *Mechanical Systems and Signal Processing*, Vol. 87, Mar. 2017, pp. 118–137.
doi:10.1016/j.ymssp.2015.10.021.

[8] Falck, R. D., Ingraham, D., Aretskin-Hariton, E., and Berton, J., "Multidisciplinary Optimization of Urban-Air-Mobility Class Aircraft Trajectories with Acoustic Constraints," *2018 AIAA/IEEE Electric Aircraft Technologies Symposium*, AIAA Propulsion and Energy Forum, Cincinnati, OH, July 2018.
doi:10.2514/6.2018-4985, AIAA 2018-4985.

[9] Bryson, A. E., and Ho, Y. C., *Applied Optimal Control: Optimization, Estimation and Control*, Rev. ed., Taylor & Francis Group, New York, 1975.
doi:10.1002/aic.690220534.

[10] Fredericks, W. J., McSwain, R. G., Beaton, B. F., and Klassman, D. W., "Greased Lightning (GL-10) Flight Testing Campaign," NASA-TM-2017-219643, NASA Langley Research Center, Hampton, VA, July 2017.

[11] Rothhaar, P. M., Murphy, P. C., Bacon, B. J., Gregory, I. M., Grauer, J. A., Busan, R. C., and Croom, M. A., "NASA Langley Distributed Propulsion VTOL Tilt-Wing Aircraft Testing, Modeling, Simulation, Control, and Flight Test Development," *14th AIAA Aviation Technology, Integration, and Operations Conference*, AIAA Aviation Forum, Atlanta, GA, June 2014.
doi:10.2514/6.2014-2999, AIAA 2014-2999.

[12] Busan, R. C., Rothhaar, P. M., Croom, M. A., Murphy, P. C., Grafton, S. B., and O'Neal, A. W., "Enabling Advanced Wind-Tunnel Research Methods Using the NASA Langley 12-Foot Low Speed Tunnel," *14th AIAA Aviation Technology, Integration, and Operations Conference*, AIAA Aviation Forum, Atlanta, GA, June 2014.
doi:10.2514/6.2014-3000, AIAA 2014-3000.

[13] Cichella, V., Xargay, E., Dobrokhodov, V., Kaminer, I., Pascoal, A. M., and Hovankimyan, N., "Geometric 3D Path-Following Control for a Fixed-Wing UAV on SO(3)," *2011 AIAA Guidance, Navigation and Control Conference*, AIAA, Portland, OR, Aug. 2011.
doi:10.2514/6.2011, AIAA 2011-6415.

[14] The MathWorks, Inc., "Simulink Ver. 8.9 (R2017a)," Natick, MA, 2017.

[15] Pascioni, K. A., and Rizzi, S. A., "Tonal Noise Prediction of a Distributed Propulsion Unmanned Aerial Vehicle," *2018 AIAA/CEAS Aeroacoustics Conference*, AIAA Aviation Forum, Atlanta, GA, June 2018.
doi:10.2514/6.2018-2951, AIAA 2018-2951.

[16] Gutin, L. Ya., "On the Sound Field of a Rotating Propeller," NACA-TM-1195, Langley Aeronautical Laboratory, Langley Field, VA, Oct. 1948.

[17] Deming, A. F., "Propeller Rotation Noise Due to Torque and Thrust," *J. Acoust. Soc. Am.*, Vol. 12, No. 1, July 1940, pp. 173–182.
doi:10.1121/1.1916089.

[18] Theodorsen, T., and Regier, A. A., "The Problem of Noise Reduction with Reference to Light Airplanes," NACA-TN-1145, Langley Aeronautical Laboratory, Langley Field, VA, Aug. 1946.

[19] Marte, J. E., and Kurtz, D. W., "A Review of Aerodynamic Noise From Propellers, Rotors, and Lift Fans," JPL-TR-32-1462, Jet Propulsion Laboratory, California Institute of Technology, Pasadena, CA, Jan. 1970.

[20] Hubbard, H. H. (ed.), *Aeroacoustics of Flight Vehicles: Theory and Practice: Volume 1: Noise Sources: NASA-RP-1258-VOL-1*, NASA Langley Research Center, Hampton, VA, 1991.

[21] Magliozzi, B., Hanson, D. B., and Amiet, R. K., "Propeller and Propfan Noise," *Aeroacoustics of Flight Vehicles: Theory and Practice: NASA-RP-1258-VOL-1*, edited by H. H. Hubbard, NASA Langley Research Center, Hampton, VA, 1991, pp. 1–64.

[22] Zorumski, W. E., and Weir, D. S., "Aircraft Noise Prediction Program Theoretical Manual: Propeller Aerodynamics and Noise," NASA-TM-83199-PT-3, NASA Langley Research Center, Hampton, VA, June 1986.

[23] Galles, M. B., "Noise Reduction of Unmanned Aerial Vehicles by Flight Control System Augmentation," M.S. Thesis, Dept. of Mechanical & Aerospace Eng., Old Dominion Univ., Norfolk, VA, Aug. 2019.

[24] Pontryagin, L. S., Boltyanskii, V. G., Gamkrelidze, R. V., and Mishchenko, E. F., *Mathematical Theory of Optimal Processes*, Interscience, New York, 1962.

[25] Kelly, M., "An Introduction to Trajectory Optimization: How to Do Your Own Direct Collocation," *SIAM Review*, Vol. 59, No. 4, Nov. 2017, pp. 849–904.
doi:10.1137/16M1062569.